Geomorphology 224 (2014) 192–202

Contents lists available at ScienceDirect

Geomorphology

journal homepage: www.elsevier.com/locate/geomorph

Application of LiDAR and discriminant analysis to determine landscape characteristics for different types of slope failures in heavily vegetated, steep terrain: Horseshoe Run watershed, West Virginia

Kory M. Konsoer [a,*], J. Steven Kite [b]

[a] Dept. of Geography and Anthropology, Louisiana State University, 227 Howe-Russell-Kniffen Geoscience Complex, Baton Rouge, LA 70803, USA
[b] Dept. of Geology and Geography, West Virginia University, 330 Brooks Hall, 98 Beechurst Ave, Morgantown, WV 26506, USA

ARTICLE INFO

Article history:
Received 3 October 2013
Received in revised form 21 June 2014
Accepted 23 June 2014
Available online 14 July 2014

Keywords:
Landslide inventory maps
LiDAR
Discriminant analysis
Natural hazards
Slope failure assessment

ABSTRACT

A landslide inventory map was created for Horseshoe Run watershed, West Virginia, using high-resolution topographic data obtained from airborne LiDAR. A total of 152 landslides were remotely mapped and classified as planar slides, rotational slumps, debris flows, debris fans, debris slides, and active slopes based on morphologic characteristics interpreted from LiDAR-derived shaded relief maps, with field verification at several locations. Seven landscape variables were calculated for the watershed from the high-resolution (0.5-m) topographic data: elevation, slope angle, slope aspect, distance from roads, distance from streams, plan curvature, and profile curvature. Statistical analyses were conducted to determine the mean and standard deviations for each variable and corresponding slope failure type. Discriminant analyses were conducted on the different types of failed slopes, with a maximum 86% accuracy level, to determine which landscape characteristics contribute to each type of landslide. Results from the discriminant analyses indicate that statistically significant differences exist between the failure classes mapped within the watershed and that slope angle, slope aspect, and landscape curvature are important variables influencing the type of process. The results from this study have important implications for predicting where certain types of slope failures may occur based on landscape characteristics.

Published by Elsevier B.V.

1. Introduction

Geologic hazards, such as landslides, are a serious threat to both life and property. In the United States alone, it is estimated that landslide hazards cause between $1 and 2 billion USD in damages and average more than 25 deaths per year (U.S. Geological Survey, 2013). The state of West Virginia is especially vulnerable to mass-wasting events given its steep topography and the effects of historic logging, mining, and other human activities (Lessing et al., 1976). Mass-wasting events can also affect watershed function by modifying stream morphology (Benda and Dunne, 1997; Cenderelli and Kite, 1998; Harvey, 2001; Michaelides and Wainwright, 2002; Hoffman and Gabet, 2007), altering local biologic populations (Vannote et al., 1980; Kreutzweiser et al., 2005; Rabeni et al., 2005), and influencing the overall landscape of a region (Downs and Gregory, 1994; Cendrero and Dramis, 1996). Understanding the factors that control slope failure is therefore invaluable in the monitoring, prediction, and mitigation of mass-wasting events, as well as contributing to models of landscape evolution.

Traditional means of evaluating landslide risk are accomplished by compiling landslide inventories and susceptibility maps. Inventory maps show the location, spatial distribution, and if available, the type and age of previously failed slopes in a given area. Depending upon the areal extent and scaling, different techniques of mapping landslides can be applied, yet typically rely on aerial photography, remote sensing, and field verification (Guzzetti et al., 2012). Susceptibility maps are then produced by using the landslide inventories and associated statistical characteristics of the landscape to determine those areas that are more prone to failure (Baeza and Corominas, 2001).

Landslide risk assessments are generally carried out for relatively large areas, where steep slopes and vegetation make it logistically difficult to rely on traditional field mapping techniques (Downing et al., 2007). In these situations, aerial photography can be utilized, however discerning between the morphologic characteristics of the type of slope failure becomes more challenging. Therefore, landslide susceptibility maps commonly combine different types of slope failures into one category, subsequently comparing landscape characteristics of simply failed to unfailed slopes.

Although these types of studies are important for overall slope stability analyses and property protection, they do not provide a means to distinguish between the different types of slope failures and the landscape characteristics that influence their occurrence. Discerning between different types of slope failures is desirable

* Corresponding author.
E-mail addresses: kkonsoer@lsu.edu (K.M. Konsoer), jkite@wvu.edu (J.S. Kite).

http://dx.doi.org/10.1016/j.geomorph.2014.06.030
0169-555X/Published by Elsevier B.V.

since the impact zone, volume, type of material, and degree of saturation can vary greatly between classes (Varnes, 1978; Campbell et al., 1985; Hungr et al., 2001). In addition, differentiation of slope processes has implications for developing landscape evolution models and stream restoration projects. The ability to produce these types of detailed inventory maps for large areas, in a time-efficient manner, has only recently been made possible by the advancement of remote sensing technologies, such as airborne light detection and ranging (LiDAR).

LiDAR-based mapping of surficial geology provides a very powerful tool for identifying the variety of surficial deposits and landforms found in diverse landscapes (Schultz, 2007). LiDAR surveys are extremely accurate and have the ability to provide high-resolution data for relatively large study areas, thereby reducing the amount of field time and allowing for observations of landforms that may otherwise be indiscernible in the field (Downing et al., 2007; Konsoer, 2008). These high-resolution, LiDAR-derived elevation models give trained users the capability of identifying different types of slope movements based on their morphologic expression.

In this study, a landslide inventory map was created using field observations and remote mapping from LiDAR-derived shaded relief maps for Horseshoe Run watershed, West Virginia. Landslides were classified as planar slides, rotational slumps, debris flows, debris fans, debris slides, or active slopes based on predefined morphologic characteristics. For each landslide mapped, seven landscape variables were determined: elevation, slope angle, slope aspect, distance from roads, distance from streams, plan curvature, and profile curvature. Statistical analyses were performed on the data to determine mean and standard deviations for each variable and corresponding slope failure type. In addition, discriminant analyses of the different classifications of failed slopes were performed, with an upper level of accuracy ~86%. The results from this study indicate that slope angle, slope aspect, and proximity to streams are important factors influencing the type of slope failure and are most likely related to the underlying structural geology and microclimate.

2. Study area

Horseshoe Run watershed is located in Tucker and Preston counties, West Virginia. The stream is ~27.2 km in length and drains an area of about 143.7 km^2 (Fig. 1). The watershed is located in heavily vegetated, steep terrain of the Allegheny Mountain section of the Appalachian Mountains; and roughly 61% of the watershed is privately owned, with the remainder lying in the Monongahela National Forest. Horseshoe Run's headwaters begin at an elevation of about 1078 m and descend nearly 637 m before draining into the Cheat River. Land use in the wide valley bottom of the lower watershed is primarily devoted to pasture, whereas the hillslopes and ridges are mainly second- or third-growth forests (Reger et al., 1923). The timber industry has a long history within the watershed that dates back to as early as 1825 (Fansler, 1962).

The overall bedrock structure of the watershed is dominated by the NE–SW trending Deer Park anticline (Cardwell et al., 1968), a broad fold with regional strike of N. 38° E. and limbs dipping at about 14° NW and SE on the flanks of the watershed (Fig. 2). Much steeper dips occur locally on numerous unmapped minor folds. Along the southeastern boundary of Horseshoe Run watershed, the resistant Pennsylvanian Pottsville sandstone comprises the ridge-forming lithology for Backbone Mountain. Mississippian units below the Pottsville sandstone include the shaley the Mauch Chunk Group (~178 m), the Greenbrier limestone (~50 m), and the resistant Pocono sandstone (~38 m), which overlies

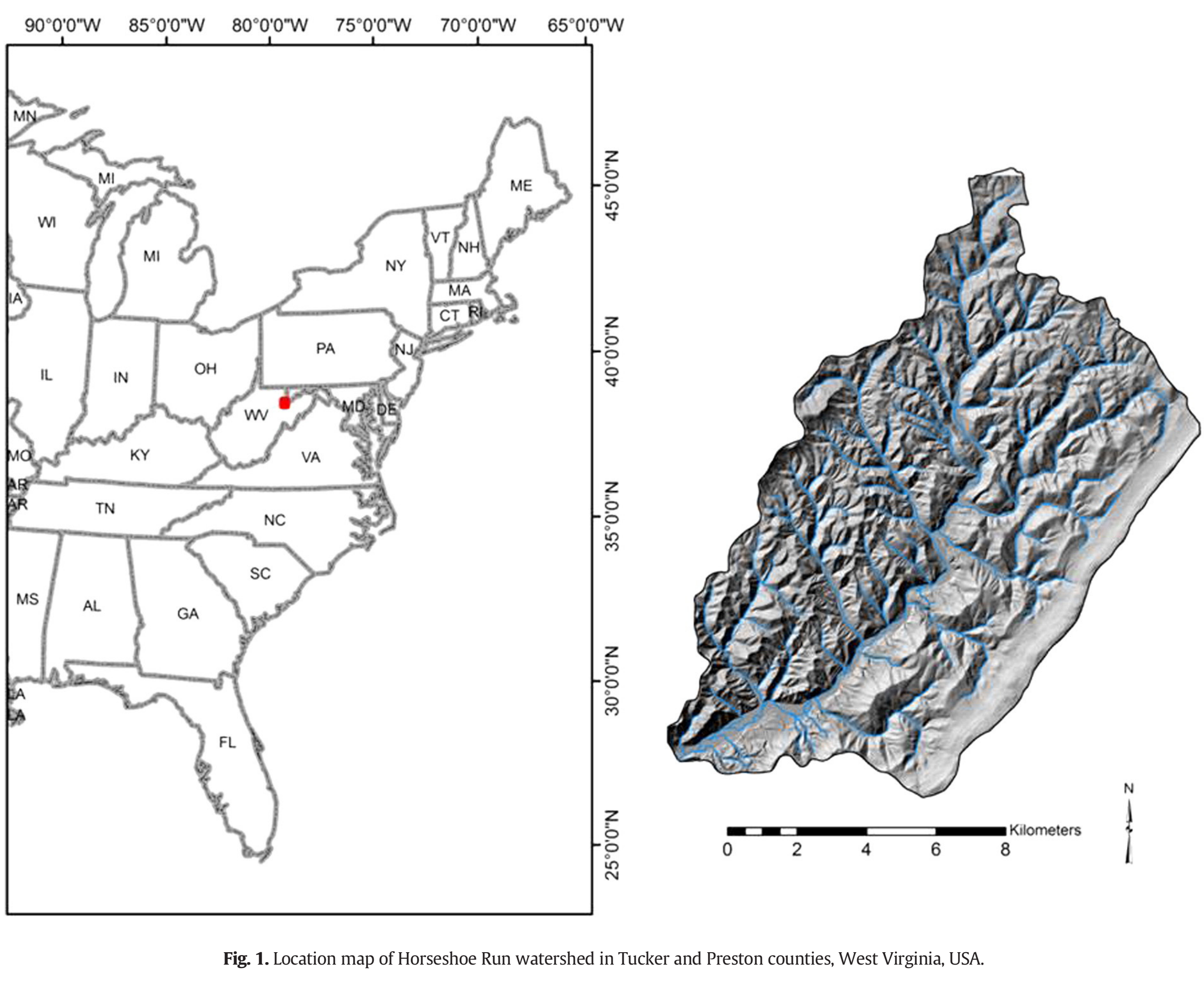

Fig. 1. Location map of Horseshoe Run watershed in Tucker and Preston counties, West Virginia, USA.

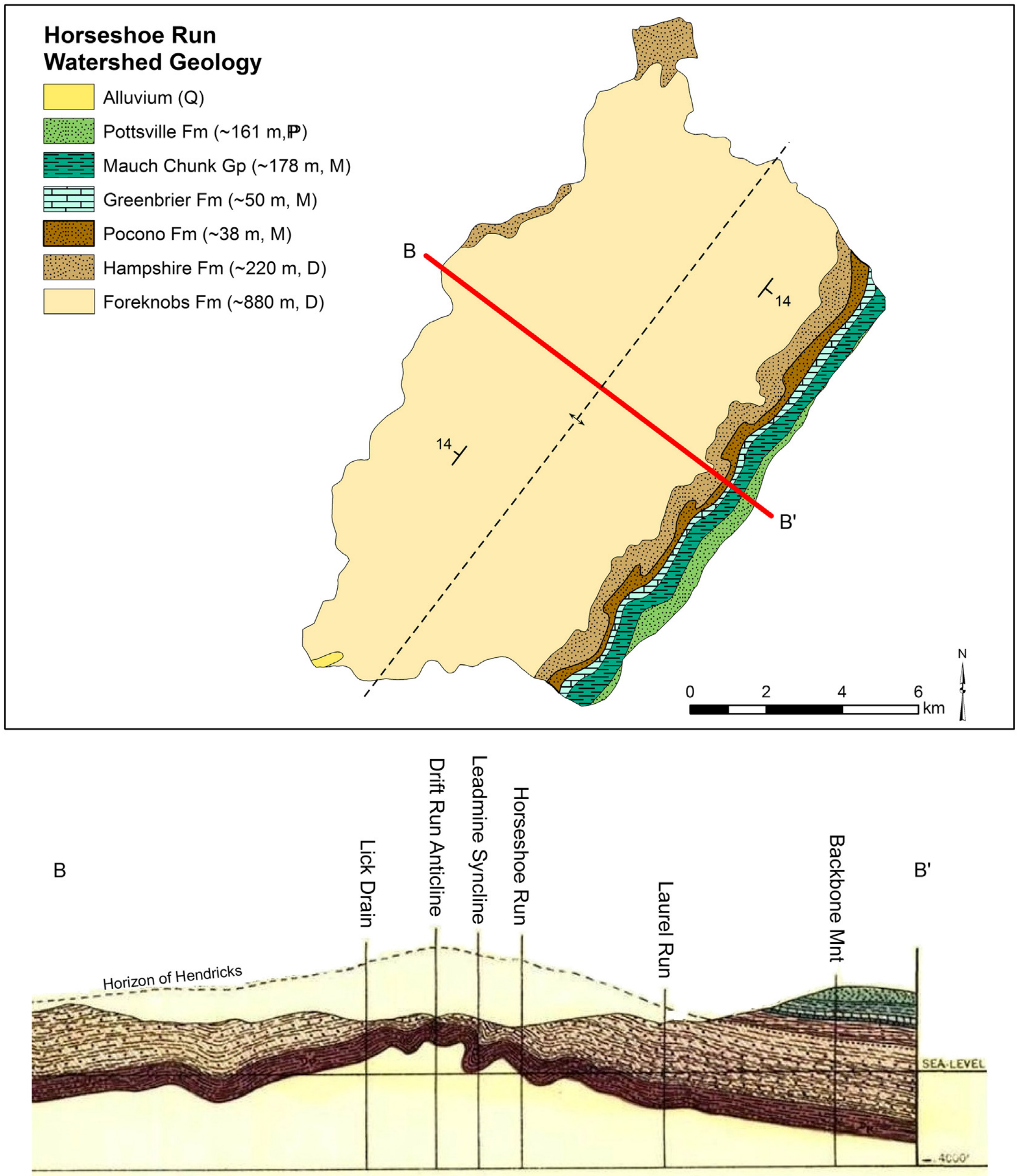

Fig. 2. Top: Bedrock geology map of Horseshoe Run watershed, West Virginia. Geologic formations are given with approximate thickness and geologic age in parentheses. Dashed line indicates approximate axial line of the Deer Park anticline. Bottom: Cross-sectional view of the structural geology of Horseshoe Run watershed showing a broad, breached anticlinal structure.
Modified from Reger et al. (1923).

the Hampshire Formation (~220 m) (Cardwell et al., 1968; Boswell, 1988). Underlying the Hampshire Formation are interbedded sandstone and shale units of the Foreknobs Formation (~880 m) (Dennison, 1970), which covers 82% of the watershed surface (Fig. 2) and has a significant influence on the surficial geology of Horseshoe Run watershed. The top of the Foreknobs Formation is marked by conglomeratic facies of the Hendricks sandstone (Reger et al., 1923). The majority of hillslope failures in the study area occur in matrix-rich colluvial diamictons derived from the Foreknobs Formation.

3. Methods

3.1. LiDAR acquisition and post-processing

The heavily vegetated terrain of Horseshoe Run watershed, with an average hillslope gradient of ~25°, makes traditional field mapping techniques logistically unfeasible; and therefore aerial LiDAR was used as the primary means to remotely map geomorphic features within the watershed. High-resolution LiDAR data and aerial photographs were obtained by the Canaan Valley Institute (CVI, 2007) via an Optech ALTM 3100 sensor and an integrated 3 band digital camera (J. Bennett, CVI, personal communication, 2007). Data acquisition was conducted in 2006 during leaf-off conditions at a flight altitude of 3500 m above ground level at an air speed of 250 km/h (135 knots) (P. Kinder, CVI, personal communication, 2008). Additionally, the pulse frequency of the sensor was set at 70 kHz with a half scan angle of 20° and a scanning frequency of 35 kHz. Flight plans were designed with 50% overlap in the swaths and a maximum of four waveform returns. The acquisition of LiDAR data enabled the creation of a DEM with 0.5-m average resolution and ~15-cm vertical accuracy (A. Greene, CVI, personal communication, 2008).

Post-processing of the LiDAR data to create a 0.5-m DEM was conducted by CVI. From the bare-earth elevation model, shaded relief maps were created using ArcGIS Spatial Analyst, which served as the base map for both field observations and remotely mapped surficial features. Hillshade maps were systematically created by maintaining a sun altitude of 45° and incremental azimuths of 45°, 135°, 225°, and 315°. The azimuth variation was aligned with regional structural trends and proved useful in highlighting surface features according to aspect.

3.2. Landslide inventory map

A landslide inventory map was constructed at a 1:12,000 scale using field observation, aerial photographs, and visual inspection of the LiDAR-derived shaded relief maps. Individual slope failures were delineated on the latter by mapping at a scale of 1:3000. Six different types of slope failures were identified within Horseshoe Run watershed based on a classification scheme modified from Varnes (1978), Campbell et al. (1985), and Hungr et al. (2001). Landform classes include: (i) debris fans, (ii) debris flows, (iii) debris slides, (iv) planar slides, (v) rotational slumps, and (vi) active slopes (Table 1; Fig. 3). Slope failure categories were inferred from the expression of landforms on the LiDAR-derived shaded relief maps, particularly, surface morphology, head scarps, displacement of slope material, and relative surface roughness (Table 1). Classified features were field checked in order to verify the diagnostic characteristics.

Debris fans are comprised of unconsolidated material commonly located on floodplains or terraces directly below tributary hollows, most showing evidence of a debris tail (Fig. 3A). *Debris flows* were mapped separately from debris fans where deposits were confined within a tributary hollow, as characterized by gravel levees, lobate margins, and lack of fan geometry (Fig. 3B). *Debris slides* were mapped where relatively coarse-grained, unconsolidated material is confined within broad hillslope hollows, having lobate or hummocky topography and little or no morphologic evidence of fluid-like flow (Fig. 3C). *Planar slides* were mapped where relatively uniform intact blocks displayed translational slide tracks with pronounced head scarps and displayed relatively less surface roughness as compared to debris slides. The mapped planar slides moved relatively short distances downslope, lacked hummocky topography, and displayed no signs of a slide toe (Fig. 3D). *Rotational slumps* are associated with hummocky topography, secondary scarps within the failure, and have a well-defined slide toe at the base of the failure (Fig. 3E). Slumps generally display less well-defined head scarps than planar slides, suggesting more of a vertical head scarp failure rather than a lateral displacement as observed in the planar slides (Figs. 3D, E). Lastly, *active slopes* were classified where unstable ground is actively moving from oversteepening and undercutting by stream channels (Fig. 3F).

Table 1
Geomorphic characteristics used to classify and map the different types of slope failures within Horseshoe Run watershed.

Type of slope failure	Characteristics used to delineate and map feature
Debris fans	Unconsolidated material confined to tributary hollows. Debris material transported to base of hillslope with a well-defined depositional fan present.
Debris flows	Unconsolidated material confined to tributary hollows with evidence of fluid-like flow. Debris material not transported to base of hillslope and still remains confined in hollows.
Debris slides	Planar slide of unconsolidated material confined to hillslope hollows. Debris slides lack well-defined depositional fans and display irregular and hummocky topography.
Planar slides	Intact blocks with significant head scarps with lateral displacement. Slide material appears uniform and lacks hummocky topography and a clearly defined slide toe.
Rotational slumps	Landslides having lobate and hummocky topography in the toe region of the slide and a visible head scarp.
Active slopes	Slopes actively moving from oversteepening and undercutting by active channels.

For purposes of analysis, the six slope failure types were aggregated into three broader groups based on association of processes, including (i) *debris* composed of debris fans, debris flows, and debris slides; (ii) *intact slides* composed of planar slides and rotational slumps; and (iii) *active slopes*. These three groups highlight differences in level of water saturation, degree of material consolidation, and triggering mechanisms (Campbell et al., 1985; Hungr et al., 2001).

To determine the conditions promoting slope failure, initiation points were identified for each class through visual inspection of head scarps, erosional surfaces, and slope breaks on hillslope profiles. These initiation points were then buffered, using a 4-m buffer tool within ArcGIS, to create polygons for data extraction. The buffering procedure was designed to reduce bias caused by using values from a single cell and to minimize potential positional error associated with LiDAR elevation data. The LiDAR-derived DEM was then resampled to create a 2-m grid from the original 0.5-m bare-earth data. This transformation reduced the size of the topographic data set and facilitated rapid calculations within ArcGIS, without sacrificing resolution required to produce a 1:12,000 scale map. The resulting initiation zone polygons consisted of ~14 raster cells used as a mask, from which average values of key landscape variables were calculated.

3.3. Multivariate statistical analyses

To identify controlling factors associated with slope failure initiation zones, seven landscape metrics were derived from the elevation models to serve as independent variables. These variables include: slope angle, slope aspect, elevation, plan curvature, profile curvature, distance from roads, and distance from streams. These landscape metrics were carefully selected for the analysis because they have been shown to influence slope failure (Baeza and Corominas, 2001; D'Amato Avanzi and Giannecchini, 2004), are directly derived from the LiDAR DEM and therefore unbiased and lack subjectivity, and are easily implemented within discriminant analyses. Slope angle and elevation are associated with potential energy in the slope material and water flow paths. Slope aspect influences soil moisture content and vegetation through variation in solar radiation. Plan curvature is a measure of topographic concavity in the horizontal plane and serves as a proxy for convergence or divergence of flow across the landscape. Profile curvature is a measure of the curvature in the vertical plane and has implications for changes in flow velocity and sediment transport (Wilson and Gallant, 2000). Distance from roads and streams was defined as the minimum linear distance, and proximity to these features can result in oversteepened slopes and instability.

Data extraction was conducted for each initiation polygon using the zonal statistics function within the Spatial Analyst extension of ArcGIS. Data outputs were combined to create subgroups based upon the type of slope failure, with subsequent statistical analyses conducted using Microsoft Excel and Minitab. Each type of slope movement was analyzed over each of the variables, except for slope aspect, to determine mean (μ), standard deviation (σ), and coefficient of variation ($c_v = \sigma / \mu$). Slope aspect data were analyzed separately from the other variables because these data are circular and occupy azimuthal space. The results of the remaining variables were used to compare between the different types of slope movements to determine if there was a statistical difference between populations. Significance between variables was tested by using the two-sample *t*-test, which tests whether two independent sample means are equal. Oriana software (Rockware, Inc.) was used to analyze the slope-aspect data and to create rose diagrams for visual comparison between the two groups.

Lastly, discriminant analyses were performed on the data split into subgroups based on type of slope failure using all seven landscape variables. Discriminant analysis is a procedure for determining boundaries between qualitative groups, such as slope failure type, in terms of the quantitative variables that characterize them (Kachigan, 1986). The analyses were designed to examine boundaries between the six

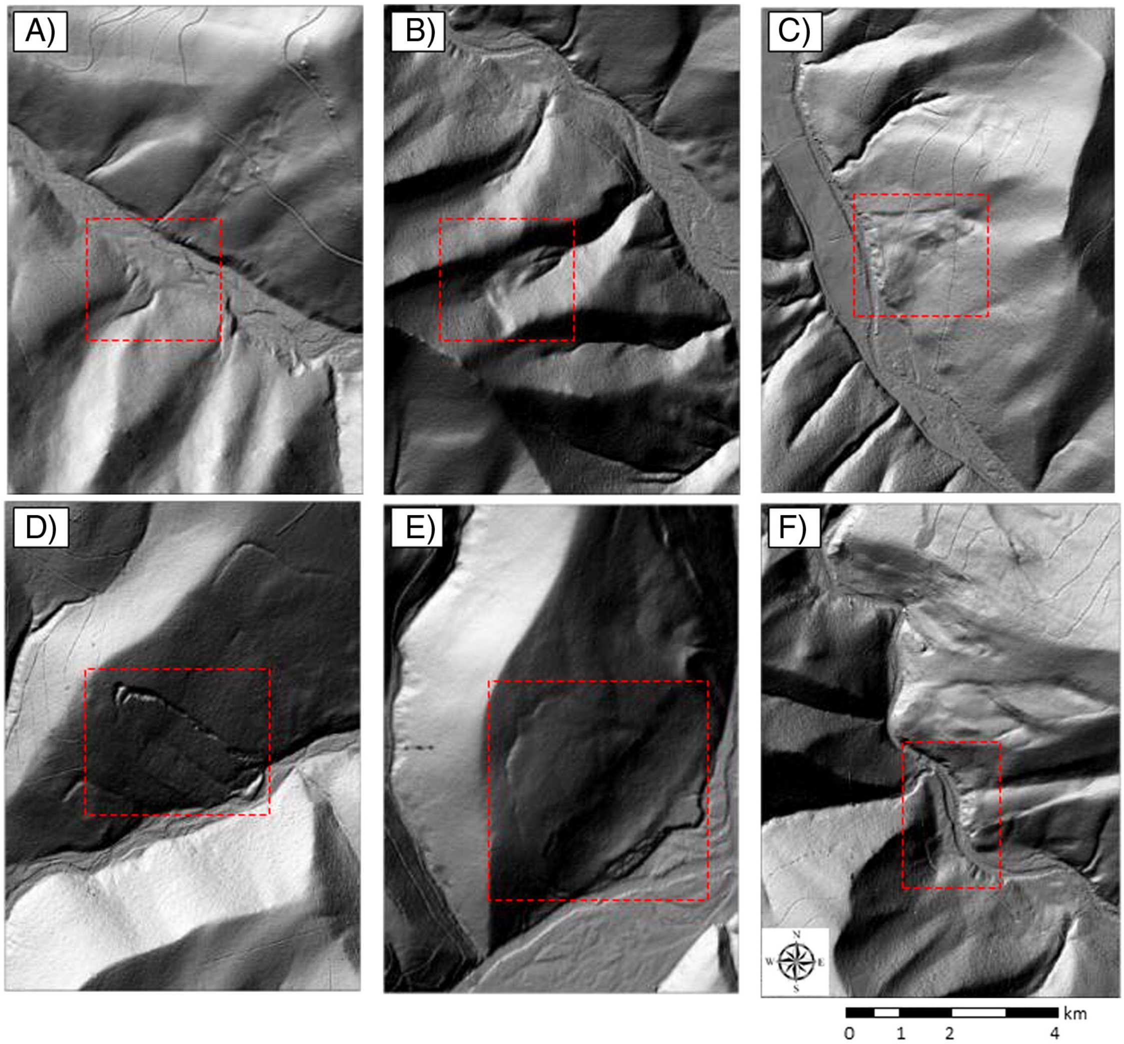

Fig. 3. Examples of the types of slope failures mapped within Horseshoe Run watershed, indicated by red squares. A) debris fan, B) debris flow, C) debris slide, D) planar slide, E) rotational slump, and F) active slopes. For morphologic characteristics, see Table 1. (For interpretation of the references to color in this figure legend, the reader is referred to the web version of this article.)

classified types of slope movements (debris fan, debris flow, debris slide, planar slide, rotational slump, and active slope) and the three general groups (debris, intact, and active).

4. Results

The landslide inventory map (Fig. 4) shows the spatial distribution of slope failures within Horseshoe Run watershed, classified according to the characteristics outlined in Table 1. Of the 152 individual slope movements mapped (Fig. 4), rotational slumps ($n = 39$) are the most abundant, followed by planar slides ($n = 38$) and active slopes ($n = 28$).

A statistical summary for the landscape variables (not including slope aspect) versus slope failure type is presented in Table 2A. Results show that the active slope class is associated with the highest mean gradient at 36° and that it occurs closest to streams with an average distance of ~61 m. The results in Table 2 also show a propensity for failures to occur on slopes that are concave in planform, signifying the importance of converging water for landslide initiation. However, as seen by the coefficients of variation, both plan and profile curvatures have the greatest relative variation for landscape variables among the different types of slope failures. In contrast, elevation and slope angle have the lowest coefficients of variation.

Comparison of statistics from the three general groups of failure types shows an even clearer distinction between the landscape variables (Table 2B). This is further demonstrated by the results of the two-sample t-tests for the three groups (Table 3). The t-test results indicate a statistically significant difference ($\alpha = 0.05$) between the slope failures classified as active slopes and the other two groups. Although not shown here, the results from the t-tests comparing all six different failure types also indicate a significant difference between the landscape variables for active slopes compared to the other failures. Additionally, the t-tests suggest a statistically significant difference between the variables of the debris group and intact group and show that values of plan curvature are similar between the active slopes and other two groups and that elevation and distance to road values are similar between the debris and intact groups.

Rose diagrams were used to evaluate azimuthal differences in slope aspect between the different types of failures. Rose plots for the three groups reveal that debris failures predominantly occur on NE-sloping landforms, whereas intact slides tend to occur on slopes sloping NW or SE (Fig. 5). Similar trends can be seen from the rose diagrams for the six different types of failures (Fig. 6). Planar slides and rotational slumps occur on slopes facing NW (or west) and SE; whereas debris fans, debris slides, and to some degree, debris flows occur mostly on slopes facing NE or SW (Fig. 6). In contrast to the other types of failures, active slopes appear to have no dominant trend in slope aspect other

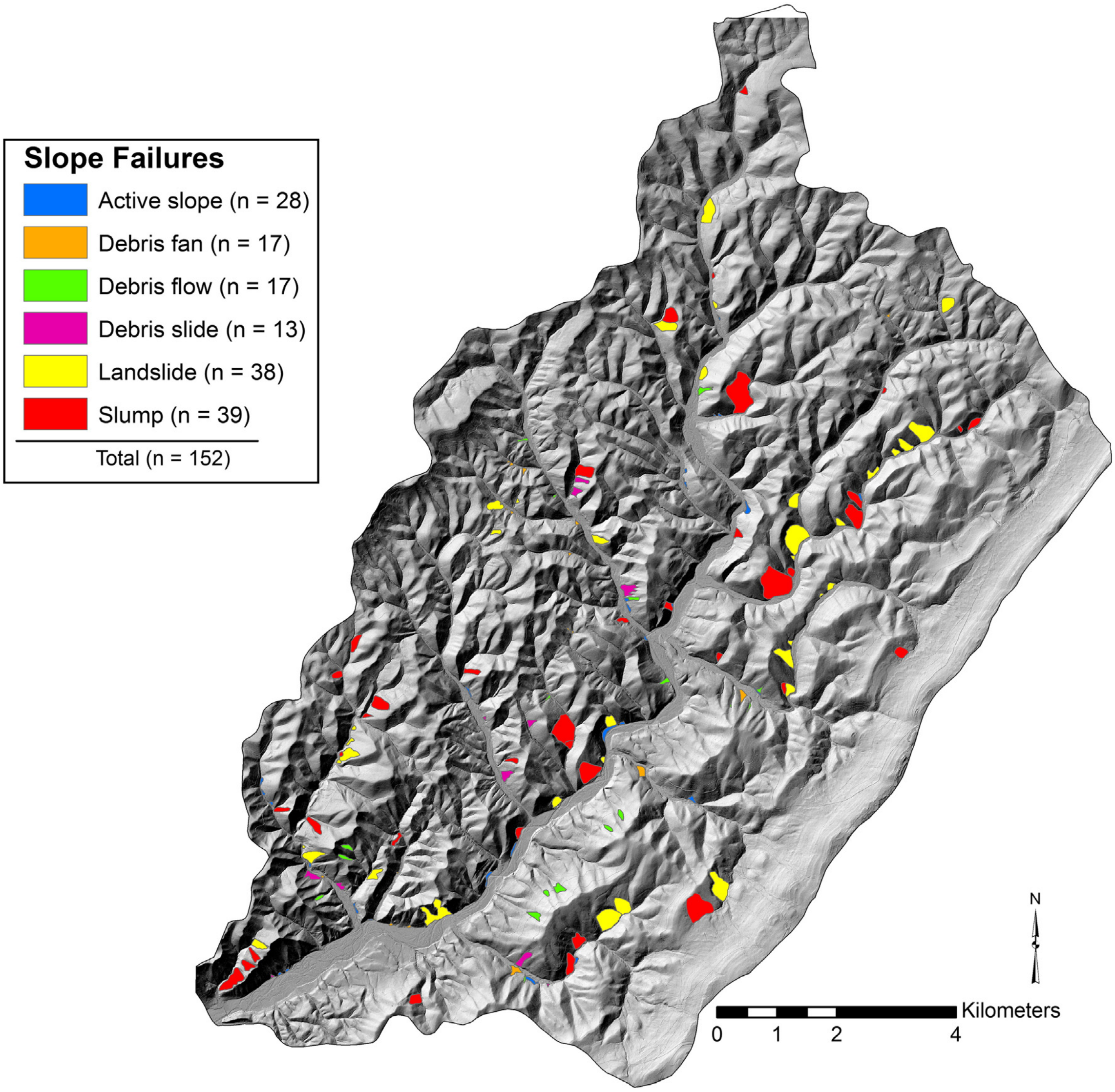

Fig. 4. Landslide inventory map showing the distribution and type of slope failures within Horseshoe Run watershed.

than a scarcity of north aspect slopes (Figs. 5 and 6). These results indicate differences in slope aspect between the specific types of slope failures as well as the general process groups of failures mapped within the watershed.

The first discriminant analysis was performed on the three groups of failures using all seven landscape variables and was 79% accurate at classifying the types of failures (Table 4). In this analysis, the circular slope aspect data were collapsed to fall between 0 and 180° (subtracting 180° from aspects >180°) in order to avoid the issue of bimodal azimuthal distribution. The coefficients from these linear discriminant functions indicate that slope angle, elevation, and plan and profile curvature are the dominate factors influencing the occurrence of a given failure class (Table 4). A second discriminant analysis was also carried out for the three groups, but instead used a quadratic classifier to

Table 2
Statistical summary for each *type* of failure class; statistical summary for different process *groups*; mean (μ), standard deviation (σ), and coefficient of variation (c_v).

		Slope angle (deg)			Elevation (m)			Plan curvature			Profile curvature			Dist. to roads (m)			Dist. to streams (m)		
Type of failure	n	μ	σ	c_v	μ	σ	c_v	μ	σ	c_v	μ	σ	c_v	μ	σ	c_v	μ	σ	c_v
Debris fan	17	26.1	5.5	0.2	662.4	45.5	0.1	−3.3	4.2	−1.3	0.5	2.8	5.7	90.7	147.1	1.6	230.5	107.8	0.5
Debris flow	17	30.3	3.1	0.1	717.2	50.1	0.1	−1.5	2.0	−1.3	0.1	1.2	17.1	115.8	112.0	1.0	440.9	167.8	0.4
Debris slide	13	32.3	4.7	0.1	625.5	71.3	0.1	0.1	2.7	24.5	−0.6	2.2	−3.6	217.8	183.9	0.8	220.7	86.8	0.4
Planar slide	38	21.8	9.2	0.4	670.4	69.5	0.1	−0.9	1.8	−1.9	1.9	2.7	1.5	139.7	136.4	1.0	210.8	99.4	0.5
Rotational slump	39	21.0	9.0	0.4	680.5	68.0	0.1	−0.4	1.3	−3.3	0.7	1.5	2.2	118.1	121.9	1.0	235.0	99.2	0.4
Active slopes	28	36.0	9.6	0.3	563.8	47.1	0.1	−1.0	2.7	−2.7	−1.7	4.5	−2.6	219.2	149.2	0.7	61.3	26.6	0.4
Process groups																			
Debris group	47	29.3	5.1	0.2	672.0	65.7	0.1	−1.7	3.4	−2.0	0.1	2.1	21.0	134.9	153.3	1.1	303.9	163.3	0.5
Intact group	77	21.4	9.0	0.4	675.5	68.5	0.1	−0.7	1.6	−2.3	1.3	2.3	1.8	128.7	128.9	1.0	223.0	99.4	0.4
Active group	28	36.0	9.6	0.3	563.8	47.1	0.1	−1.0	2.7	−2.7	−1.7	4.5	−2.6	219.2	149.2	0.7	61.3	26.6	0.4

Table 3
Two-sample t-tests comparing the landscape variables for the three different groups of slope failures at a 95% confidence level ($\alpha = 0.05$) ("X" indicates that the two samples were significantly different; "0" indicates the two samples were similar; A = active slopes; D = debris; I = intact slides).

	A/D	A/S	D/S
Slope angle	X ($t = 3.37, p = 0.002$)	X ($t = 7.18, p = 0.001$)	X ($t = 5.50, p = 0.001$)
Elevation	X ($t = -7.62, p = 0.001$)	X ($t = -7.97, p = 0.001$)	0 ($t = -0.28, p = 0.779$)
Plan curvature	0 ($t = 0.94, p = 0.353$)	0 ($t = -0.86, p = 0.390$)	X ($t = -2.30, p = 0.023$)
Profile curvature	X ($t = -2.25, p = 0.027$)	X ($t = -3.33, p = 0.002$)	X ($t = -3.03, p = 0.003$)
Dist. roads	X ($t = 2.33, p = 0.023$)	X ($t = 3.05, p = 0.003$)	0 ($t = 0.23, p = 0.818$)
Dist. streams	X ($t = -7.78, p = 0.001$)	X ($t = -8.48, p = 0.001$)	X ($t = 3.43, p = 0.001$)

distinguish between the groups and produced even better results, having an accuracy of 86% (Table 5).

A linear discriminant analysis performed on the six different types of slope failures produced less accurate results, with an accuracy of only 55% (Table 6). However, upon further inspection, the results indicate that active slopes were accurately classified 82% of the time. Furthermore, the misclassifications of the other five failure types were mostly classified within the same general failure group (Table 6). For example, the discriminant function accurately classified 14 planar slides, while 15 of the mapped planar slides were misclassified as rotational slumps. Similarly, the three different types of debris failures were most commonly misclassified as other failures within the general debris group.

The discriminant functions from the analysis performed on the six different types of failures yielded similar results to the discriminant functions for the three groups (Tables 4 and 6). For each discriminant function, slope angle and profile curvature were the most influential landscape variables determining the type of failure that would occur; elevation and plan curvature determined type of failure to a lesser extent. Conversely, slope aspect seems to have very little influence based on the discriminant function, despite the rose patterns indicating a tendency for preferred slope orientation. One possible explanation for this is the difficulty of dealing with circular data that has a strong bimodal distribution, leading to canceling effects when determining boundaries between the classifications. This is supported by performing

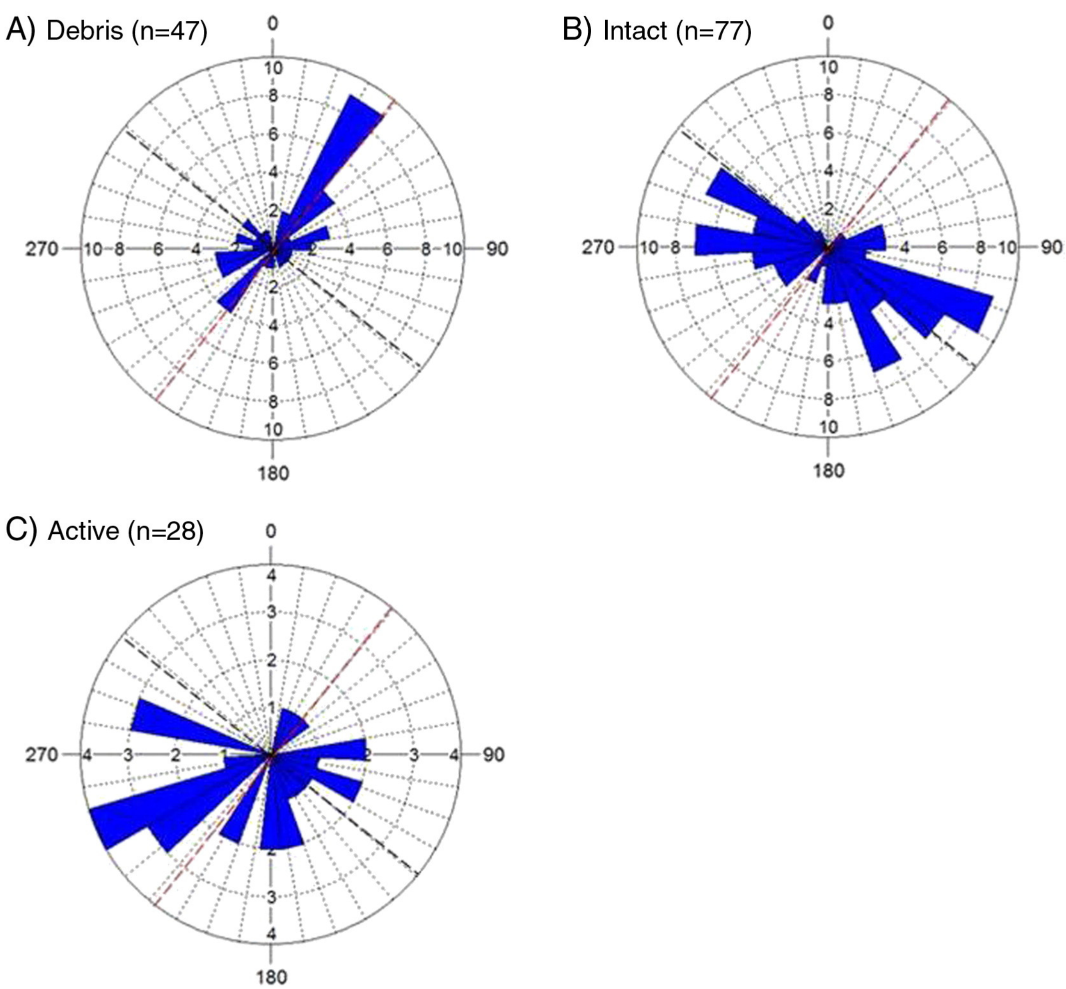

Fig. 5. Rose diagrams showing the slope aspect for the three groups of classified slope failures. Note the difference in preferred slope orientation between the debris and intact slide groups, whereas active slopes show no preferred orientation. Red dashed line represents strike of breached anticline; black dashed line represents general dip direction of bedrock. (For interpretation of the references to color in this figure legend, the reader is referred to the web version of this article.)

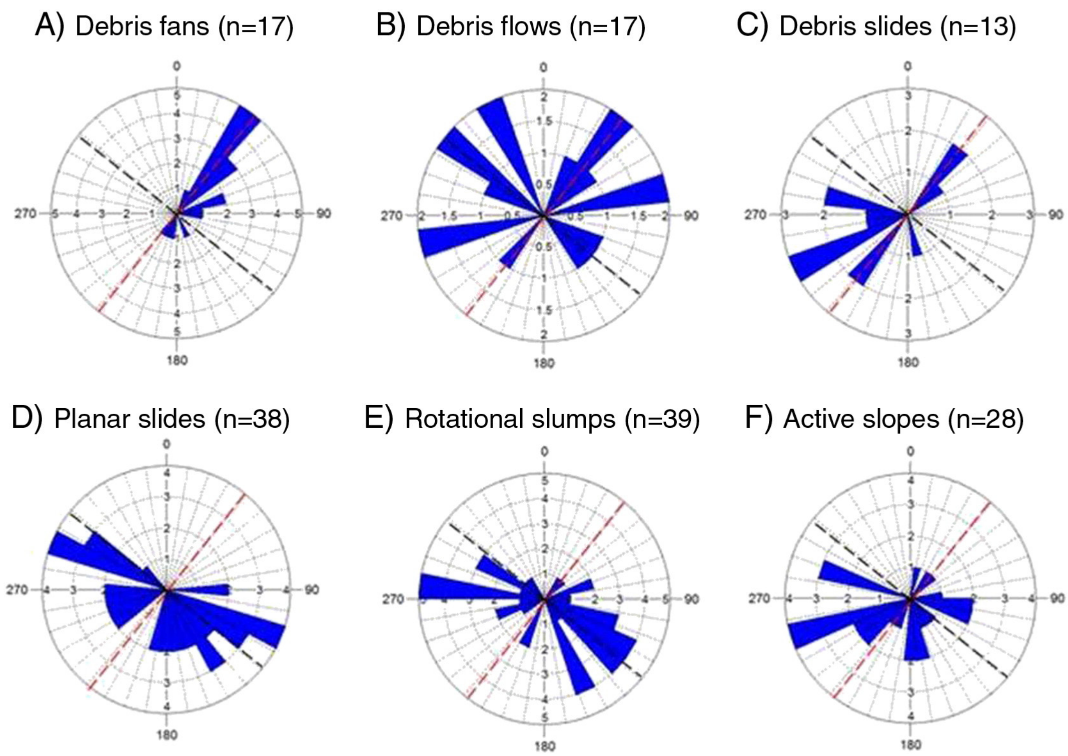

Fig. 6. Rose diagrams showing the slope aspect for the six different types of classified slope failures. Red dashed line represents strike of breached anticline; black dashed line represents general dip direction of bedrock. (For interpretation of the references to color in this figure legend, the reader is referred to the web version of this article.)

a quadratic discriminant analysis on the different types of failures, which resulted in a much higher accuracy of 74% (Table 7).

5. Discussion

From the results shown above, well-defined boundaries clearly exist between the three different groups of failures based on the landscape variables used within this study. Evidence also suggests that the six different types of slope failures mapped within this watershed have distinct boundary conditions, although some overlap between failure types within the same general group does occur. However, this overlap may be a direct consequence of the landslide classification process. The classification of landslides forces naturally occurring phenomena, which vary over a continuous spectrum, into discrete categories; and commonly, landslides are complex and have characteristics that fall into different categories simultaneously (Alexander, 2008). Nevertheless, the results give supporting evidence that the occurrence and type of slope failure are strongly dependent upon landscape parameters and the underlying geology of the watershed. Furthermore, understanding how these landscape conditions influence slope failures allows for better prediction of the type of failure to occur, with implications for the amount and type of material and the potential influence of the failure on the landscape.

The results from the discriminant analyses at Horseshoe Run watershed indicate that slope angle, elevation, plan curvature, profile curvature, and slope aspect are all primary factors influencing slope failure. Although others (D'Amato Avanzi and Giannecchini, 2004; Baeza and

Table 4
Linear discriminant analysis performed on the three groups of classified slope failures; shown are the true versus predicted classifications, the proportion of correctly classified slope failures, and the linear coefficients for the discriminant functions determined for each group.

	True		
Predicted	Debris	Intact	Active
Summary of classification			
Debris	37	16	0
Intact	6	57	2
Active	4	4	26
Total N	37	77	28
N correct	37	57	26
Proportion	0.79	0.74	0.93
N = 152; N correct = 120			
Proportion correct = 0.79			
Linear discriminant function for groups			
Constant	−110.11	−109.62	−103.63
Slope	9.2	0.81	0.96
Aspect	−0.03	−0.02	−0.01
Elevation	0.31	0.31	0.29
Plan curvature	0.37	0.62	0.17
Profile curvature	0.65	0.85	0.26
Dist. to roads	0.06	0.06	0.06
Dist. to streams	−0.06	−0.07	−0.07

Table 5
Quadratic discriminant analysis performed on the three different groups of slope failures, resulting in approximately 86% level of accuracy.

	True		
Predicted	Debris	Intact	Active
Summary of classification			
Debris	39	7	1
Intact	6	64	0
Active	2	6	27
Total N	47	77	28
N correct	39	64	27
Proportion	0.83	0.83	0.97
N = 152; N correct = 130			
Proportion correct = 0.86			

Table 6
Linear discriminant analysis performed on the six different types of classified slope failures; shown are the true versus predicted classifications, the proportion of correctly classified slope failures, and the linear coefficients for the discriminant functions determined for each type.

Predicted	True					
	Active slope	Debris fan	Debris flow	Debris slide	Planar	Slump
Summary of classification						
Debris fan	0	11	3	2	2	2
Debris flow	0	2	11	1	2	2
Debris slide	4	1	2	6	4	7
Planar	1	1	0	2	14	8
Slump	0	2	1	1	15	19
Active slope	23	0	0	1	1	1
Total N	28	17	17	13	38	39
N correct	23	11	11	6	14	19
Proportion	0.82	0.65	0.65	0.47	0.37	0.49
N = 152; N correct = 84						
Proportion correct = 0.55						
Linear discriminant function for groups						
Constant	−102.94	−106.96	−119.47	−109.31	−110.47	−109.69
Slope	0.99	0.88	1.01	0.99	0.85	0.84
Aspect	0.00	−0.02	−0.01	0.00	0.00	0.00
Elevation	0.29	0.30	0.30	0.30	0.31	0.31
Plan curvature	0.32	0.02	0.56	0.78	0.73	0.73
Profile curvature	0.34	0.59	0.84	0.74	1.01	0.86
Dist. to roads	0.06	0.05	0.06	0.06	0.06	0.06
Dist. to streams	−0.06	−0.05	−0.03	−0.05	−0.06	−0.05

Corominas, 2001) have similarly documented the influence of these factors on the overall stability of slopes, this research suggests that these factors will also influence the *type* of failure that will occur.

Slope aspect is perhaps the variable that best explains this influence. The rose diagrams indicate that the different groups of slope failures have different preferred orientations (Figs. 5 and 6). The group composed of the debris failures occurred primarily on anti-dip slopes with a NE orientation, whereas the group composed of intact slides occurred on dip slopes with a NW to SE orientation. Two possible explanations for this preferred orientation may be the orientation of the breached NE–SW anticlinal structure across the watershed (Figs. 2, 5, and 6), and differences in microclimate and soil moisture associated with structurally controlled slope aspect.

Slope failures commonly fail initially along bedding planes where the underlying bedrock is dipping in the downslope direction (Jacobson et al., 1987, 1989; Guzzetti et al., 1996; D'Amato Avanzi and Giannecchini, 2004). The underlying lithology will also influence the associated hillslope material and the stability of the slope (Outerbridge, 1987; Lorente et al., 2002). The presence of shaley bedrock units is commonly associated with clay-rich residuum, and if those clays are expandable, the chances of slope failure are greatly increased (Behling, 1987; Summa et al., 2010; Jeong et al., 2011). In the case of Horseshoe Run watershed, the planar slides and rotational slumps, occurring on slopes with NW and SE orientations (Fig. 5), are most likely failing along the NW- and SE-dipping beds of sandstone and shale in the Foreknobs Formation associated with the breached Deer Park anticlinal structure as suggested by the rose patterns (Figs. 5 and 6). In contrast, the debris-style failures are predominantly occurring on anti-dip slopes with NE slope aspect. Additionally, a large proportion of planar slides and rotational slumps occur on the more gently dipping flanks for the anticline, while debris-style failures are mostly observed on anti-dipping slope near the center of the watershed along the axial fold of the anticline (Fig. 4).

The strong structural signature of the watershed could also be affecting the microclimate by influencing the amount of solar radiation, type of vegetation, and thereby amount of soil moisture on slopes with varying aspect (Bennie et al., 2008). In the northern hemisphere, south-facing slopes receive more solar radiation than the north-facing slopes, and therefore results in warmer temperatures and greater rates of evapotranspiration (Hack and Goodlett, 1960). In contrast, slopes with NE aspect within Horseshoe Run watershed receive lower amounts of heating from solar radiation because they receive solar rays during the morning hours when temperatures are cool, as opposed to slopes with NW and south aspect which receive solar rays during the afternoon when temperatures are warmer. These inferred differences in microclimate, evapotranspiration rates, and soil moisture could also be partly responsible for the prevalence of debris-style slope failures occurring on anti-dip slopes with NE orientations (Figs. 5 and 6).

The vast majority of hillslope failures in Horseshoe Run watershed occur within the interbedded sandstone and shale of the Foreknobs Formation. This is most likely because most of the watershed is underlain by the Foreknobs Formation (~82% of surface area within the watershed) and karst development in the Greenbrier limestone outcrop belt acting as a sink for colluvium originating from Pottsville sandstone outcrops at the very highest elevations in the watershed. Furthermore, the Pottsville sandstone is more resistant to erosion; and the weathering products from this formation are mostly large boulders of coarse sandstone, particles which are less likely to generate slope failures than finer grained regolith (Hack and Goodlett, 1960). Downslope transportation of Pottsville-derived boulders tends to occur as very local rock fall and exceedingly slow creep, such that large boulders physically weather into smaller clasts within 100 m of source outcrops. In contrast, weathering products of the Foreknobs sandy shales and interbedded sandstone produce poorly sorted matrix-rich colluvial diamictons, much more prone to slope failure. These diamictons are well exposed where stream channels have eroded the toes of the deposits.

The ability to differentiate between landslide *types* is desirable for many reasons. As mentioned above, the volume, type of material, and impact zone can vary between failure types, thus affecting the landscape and influencing infrastructure in different ways. As an example, the surficial extent of each mapped failure was determined within ArcGIS (Table 8). Estimates of volume were not performed because of a lack of detailed deposit thickness and porosity for each individual deposit. However, the estimates of surficial area show that the planar

Table 7
Quadratic discriminant analysis performed on the six different types of slope failures, resulting in approximately 74% level of accuracy.

Predicted	True					
	Active slope	Debris fan	Debris flow	Debris slide	Planar	Slump
Summary of classification						
Debris fan	1	13	1	0	0	2
Debris flow	0	2	16	1	2	0
Debris slide	0	0	0	12	2	3
Planar	0	1	0	0	18	6
Slump	0	1	0	0	13	27
Active slope	27	0	0	0	3	1
Total N	28	17	17	13	38	39
N correct	27	13	16	12	18	27
Proportion	0.97	0.77	0.94	0.92	0.47	0.70
N = 152; N correct = 113						
Proportion correct = 0.74						

Table 8
Mean surficial area for each type of failure class.

Type	Mean area (m^2)
Debris fan	4769
Debris flow	8709
Debris slide	15,239
Planar	33,492
Slump	33,492
Active	4719

Fig. 7. Coarse, subangular to subrounded cobbles in a debris flow deposit in Horseshoe Run watershed.

slides and rotational slumps mapped within Horseshoe Run watershed are an order of magnitude larger than debris fans, debris flows, and active slopes. Additionally, observations of slope failures in the field verify that debris fans and debris flows were composed of very coarse bouldery deposits (Fig. 7).

Lastly, the results from this study highlight the utility of incorporating LiDAR elevation data with GIS and statistical analyses to document and predict the type of slope failure that will occur given various landscape metrics. The availability of high-resolution LiDAR data, the increasing versatility of GIS, and the ability to integrate multiple factors have clearly influenced the current trend of research toward using statistical spatial analyses in landslide risk assessments (e.g., Carrara et al., 1999; Guzzetti et al., 1999; Rickenmann, 1999; Baeza and Corominas, 2001; Dai and Lee, 2002; He et al., 2003; Ohlmacher and Davis, 2003; Guzzetti et al., 2005). However, the findings presented in this paper address the ability to predict failure type based solely on landscape characteristics near initiation zones. These techniques could be further developed to determine the landscape characteristics and slope failure properties that are important for determining debris flow runout and depositional zones (Benda and Cundy, 1990; Rickenmann, 1999).

Researchers should be cautious and understanding of the limitations and assumptions associated with these approaches to landslide studies, and models of landslide susceptibility should be carefully calibrated against a particular area of interest. Bias and subjectivity are two of the major concerns identified by many researchers (Guzzetti et al., 2000; Carrara et al., 2008; Galli et al., 2008; Guzzetti et al., 2012). This can be the result of: (i) converting qualitative variables, such as underlying geologic formations or soil types, into quantitative variables; (ii) absent or improper use of statistical analyses of the input parameters; and (iii) misinterpretation of the geomorphic expression of slope failures by untrained users. The introduced bias and subjectivity can lead to poor quality landslide or landscape data (Carrara and Pike, 2008). The quality assurance issue supports the assertion by Galli et al. (2008) that inferior observations are commonly gathered quickly in order to apply the data manipulation and multivariate statistical analyses that are so easily conducted within GIS. Sophistication of technology and methods cannot, however, compensate for substandard input data (Carrara and Pike, 2008); and inappropriate use of such models can have negative consequences to human life and property.

6. Conclusions

Slope failures mapped within Horseshoe Run watershed using field observations, aerial photography, and LiDAR elevation models are subdivided into six different *types* and into three different *groups* of failures based on morphological characteristics. Of the 152 mapped failures, the intact slide group (77) was the most abundant, followed by the debris group (47) and active slopes (28). Similarly, rotational slumps (39) and planar slides (38) were the most commonly mapped type of slope failure within Horseshoe Run watershed. Given the steep topography and heavy vegetation, use of 0.5-m LiDAR-derived shaded relief maps was essential in accurately delineating slope failures within this Appalachian watershed.

Statistical analyses performed on the different types and groups of failures indicate that statistically significant differences exist between the features mapped within the watershed. The results from two-sample *t*-tests and rose diagrams show that slope angle and slope aspect had the greatest variation between classified failure groups and types of the seven landscape variables used in this study, emphasizing the importance of the underlying geology within the watershed. Results from the *t*-tests also show that failures classified as active slopes were significantly different from the others across all seven landscape variables, clearly indicating slope process differences between the groups. Distance to roads and streams were the most similar variables among the types of failures, suggesting that these two parameters had very limited influence on the type of slope failure.

The quadratic discriminant analysis performed on the three groups of failures further validated the two-sample *t*-tests showing that the boundaries between the groups were well defined and could be classified with an 86% level of accuracy. On the other hand, the linear discriminant analysis of the six different types of failures only had an accuracy level of 55%. However, for each type of slope failure, the misclassified features typically were predicted from within the same general failure group. The accuracy levels suggest that the groups of classified slope failures are influenced by similar physical processes and landscape variables and that the overlap between the different failure types should not be interpreted as errors as much as an artifact of bin classification of continuously varying natural phenomena. Yet despite this apparent overlap, the discriminant functions were fairly consistent and in agreement with the *t*-tests that slope angle, elevation, slope aspect, and curvature are important landscape variables affecting the occurrence and type of slope failures within the Horseshoe Run watershed. As such, the results from this study might not be appropriate for other watersheds; however, the method present within this paper could be similarly applied to other watersheds and landscapes.

Acknowledgments

The authors would like to thank Beau Downing, Keri Wilson, and David Bennett for their assistance with the landslide mapping inventory. We would also like to thank the Canaan Valley Institute for providing the LiDAR data for this research. Supported by the U. S. Geological Survey, National Cooperative Geologic Mapping Program, under assistance Award No. 07HQAG0059. The views and conclusions contained in this document are those of the authors and should not be interpreted as necessarily representing the official polices, either expressed or implied, of the U.S. Government. Funding for this research was also provided through a Geological Society of America graduate student research grant 1818-07. This manuscript was greatly improved from reviews by Dr. Steven Taylor, Dr. Richard Marston, and three anonymous reviewers.

References

Alexander, D.E., 2008. A brief survey of GIS in mass-movement studies, with reflections on theory and methods. Geomorphology 94 (3–4), 261–267.
Baeza, C., Corominas, J., 2001. Assessment of shallow landslide susceptibility by means of multivariate statistical techniques. Earth Surf. Process. Landf. 26 (12), 1251–1263.
Behling, R.E., 1987. Slope instability in the Appalachian Plateaus Province, West Virginia: numerous cases, numerous causes, few cures. Landslides of Eastern North America. U.S. Geological Survey Circular 1008, Norfolk, VA, pp. 35–36.
Benda, L., Cundy, T.W., 1990. Predicting deposition of debris flows in mountain channels. Can. Geotech. J. 27 (4), 409–417.

Benda, L., Dunne, T., 1997. Stochastic forcing of sediment supply to channel networks from landsliding and debris flow. Water Resour. Res. 33 (12), 2849–2863.
Bennie, J., Huntley, B., Wiltshire, A., Hill, M.O., Baxter, R., 2008. Slope, aspect and climate: spatially explicit and implicit models of topographic microclimate in chalk grassland. Ecol. Model. 216 (1), 47–59.
Boswell, R., 1988. Stratigraphic expression of basement fault zones in northern West Virginia. Geol. Soc. Am. Bull. 100 (12), 1988–1998.
Campbell, R.H., Varnes, D.J., Fleming, R.W., Hampton, M.A., Prior, D.B., Sangrey, D.A., Nichols, D.R., Brabb, E.E., 1985. Landslide classification for identification of mud flows and other landslides. In: Campbell, R.H. (Ed.), Feasibility of a Nationwide Program for the Identification and Delineation of Hazards From Mud Flows and Other Landslides: U.S. Geological Survey Open-File Report 85-276, Reston, VA, pp. A1–A24.
Cardwell, D.H., Erwin, R.B., Woodward, H.P., 1968. Geologic Map of West Virginia. West Virginia Geological and Economic Survey Map 1, 2 sheets, scale 1:250,000.
Carrara, A., Pike, R., 2008. GIS technology and models for assessing landslide hazard and risk: editorial. Geomorphology 94 (3–4), 257–260.
Carrara, A., Guzzetti, F., Cardinali, M., Reichenbach, P., 1999. Use of GIS technology in the prediction and monitoring of landslide hazard. Nat. Hazards 20 (2–3), 117–135.
Carrara, A., Crosta, G., Frattini, P., 2008. Comparing models of debris-flow susceptibility in the alpine environment. Geomorphology 94 (3–4), 353–378.
Cenderelli, D.A., Kite, J.S., 1998. Geomorphic effects of large debris flows on channel morphology at North Fork Mountain, eastern West Virginia, USA. Earth Surf. Process. Landf. 23 (1), 1–19.
Cendrero, A., Dramis, F., 1996. The contribution of landslides to landscape evolution in Europe. Geomorphology 15 (3–4), 191–211.
CVI, 2007. Horseshoe Run in Tucker County, West Virginia. www.canaanvi.org (data accessed February, 2007).
D'Amato Avanzi, G., Giannecchini, A.P., 2004. The influence of the geological and geomorphological settings on shallow landslides. An example in a temperate climate environment: the June 19, 1996 event in northwest Tuscany (Italy). Eng. Geol. 73 (3–4), 215–228.
Dai, F.C., Lee, C.F., 2002. Landslide characteristics and slope instability modeling using GIS, Lantau Island, Hong Kong. Geomorphology 42 (3–4), 213–228.
Dennison, J.M., 1970. Stratigraphic division of Upper Devonian Greenland Gap Group ("Chemung Formation") along the Allegheny Front in West Virginia, Maryland, and Highland County. Southeast. Geol. 12 (1), 53–82.
Downing, J., Konsoer, K.M., Kite, J.S., 2007. LiDAR based surficial geology mapping in comparison to more traditional methods in the heavily vegetated Appalachian Mountains. Geol. Soc. Am. Abstr. Prog. 39 (6), 161.
Downs, P.W., Gregory, K.J., 1994. The sensitivity of river channels in the landscape system. Landscape SensitivityJohn Wiley and Sons, Chichester, United Kingdom, pp. 15–29.
Fansler, H.F., 1962. History of Tucker County, West Virginia. McClain Printing Company, West Virginia, p. 702.
Galli, M., Francesca, A., Cardinali, M., Guzzetti, F., Reichenbach, P., 2008. Comparing landslide inventory maps. Geomorphology 94 (3–4), 268–289.
Guzzetti, F., Cardinali, M., Reichenbach, P., 1996. The influence of structural setting and lithology on landslide type and pattern. Environ. Eng. Geosci. 2 (4), 531–555.
Guzzetti, F., Carrara, A., Cardinali, M., Reichenbach, P., 1999. Landslide hazard evaluation; a review of current techniques and their application in a multi-scale study, central Italy. Geomorphology 31 (1–4), 181–216.
Guzzetti, F., Cardinali, M., Reichenbach, P., 2000. Comparing landslide maps: a case study in the upper Tiber River Basin, Central Italy. Environ. Manag. 25 (3), 247–363.
Guzzetti, F., Reichenbach, P., Cardinali, M., Galli, M., Ardizzone, F., 2005. Probabilistic landslide hazard assessment at the basin scale. Geomorphology 72 (1–4), 272–299.
Guzzetti, F., Mondini, A.C., Cardinali, M., Fiorucci, F., Santangelo, M., Chang, K.T., 2012. Landslide inventory maps: new tools for an old problem. Earth Sci. Rev. 112 (1–2), 42–66.
Hack, J.T., Goodlett, J.C., 1960. Geomorphology and forest ecology of a mountain region in the central Appalachians. U.S. Geological Survey, Professional Paper, 347 (66 pp.).
Harvey, A.M., 2001. Coupling between hillslopes and channels in upland fluvial systems: implications for landscape sensitivity, illustrated from the Howgill Fells, northwest England. Catena 42 (2–4), 225–250.
He, Y.P., Xie, H., Cui, P., Wei, F.Q., Zhong, D.L., Gardner, J.S., 2003. GIS-based hazard mapping and zonation of debris flows in Xiaojiang Basin, southwestern China. Environ. Geol. 45 (2), 286–289.
Hoffman, D.F., Gabet, E.J., 2007. Effects of sediment pulses on channel morphology in a gravel-bed river. Geol. Soc. Am. Bull. 119 (1/2), 116–125.
Hungr, O., Evans, S.G., Bovis, M.J., Hutchinson, J.N., 2001. A review of the classification of landslides of the flow type. Environ. Eng. Geosci. 7 (3), 221–238.
Jacobson, R.B., Cron, E.D., McGeehin, J.P., 1987. Preliminary results from a study of natural slope failures triggered by the storm of November 3–5, 1985, Germany Valley, West Virginia and Virginia. Landslides of Eastern North America, U.S. Geological Survey Circular 1008, Norfolk, VA, pp. 11–16.
Jacobson, R.B., Cron, E.D., McGeehin, J.P., 1989. Slope movements triggered by heavy rainfall, November 3–5, 1985, in Virginia and West Virginia, U.S.A. In: Schultz, A.P., Jibson, R.W. (Eds.), Landslide Processes of the Eastern United States and Puerto Rico. Geological Society of America Special Paper, 236, pp. 1–14.
Jeong, G., Kim, K., Choo, C., Kim, J., Kim, M., 2011. Characteristics of landslides induced by a debris flow at different geology with emphasis on clay mineralogy in South Korea. Nat. Hazards 59 (1), 347–365.
Kachigan, S.K., 1986. Statistical Analysis: An Interdisciplinary Introduction to Univariate and Multivariate Methods. Radius Press, New York (589 pp.).
Konsoer, K.M., 2008. LiDAR, GIS, and Multivariate Statistical Analysis to Assess Landslide Risk, Horseshoe Run Watershed, West Virginia(M.S. Thesis) West Virginia University.
Kreutzweiser, D.P., Capell, S.S., Good, K.P., 2005. Effects of fine sediment inputs from a logging road on stream insect communities: a large-scale experimental approach in a Canadian headwater stream. Aquat. Ecol. 39 (1), 55–66.
Lessing, P., Kulander, B.R., Wilson, B.D., Dean, S.L., Woodring, S.M., 1976. West Virginia landslides and slide-prone areas. West Virginia Geological and Economic Survey Publication EGB-15a (68 pp.).
Lorente, A., Garcia-Ruiz, J.M., Begueria, S., Arnaez, J., 2002. Factors explaining the spatial distribution of hillslope debris flows: a case study in the Flysch Sector of the central Spanish Pyrennes. Mt. Res. Dev. 22 (1), 32–39.
Michaelides, K., Wainwright, J., 2002. Modeling the effects of hillslope-channel coupling on catchment hydrological response. Earth Surf. Process. Landf. 27 (1), 1441–1457.
Ohlmacher, G.C., Davis, J., 2003. Using multiple logistic regression and GIS technology to predict landslide hazard in northeast Kansas, USA. Eng. Geol. 69 (3–4), 331–343.
Outerbridge, W.F., 1987. Relation between landslides and bedrock in the central Appalachian Plateaus. Landslides of Eastern North America, U.S. Geological Survey Circular 1008, pp. 36–37.
Rabeni, C.F., Doisy, K.E., Zweig, L.D., 2005. Stream invertebrate community functional responses to deposited sediment. Aquat. Sci. 67 (4), 395–402.
Reger, D.B., Price, W.A., Tucker, R.C., 1923. Tucker County, county report. West Va. Geol. Surv. Cty. Geol. Rep. 27, 542.
Rickenmann, D., 1999. Empirical relationships for debris flows. Nat. Hazards 19 (1), 47–77.
Schultz, W.H., 2007. Landslide susceptibility revealed by LiDAR imagery and historical records, Seattle, Washington. Eng. Geol. 89 (1–2), 67–87.
Summa, V., Tateo, F., Giannossi, M.L., Bonelli, C.G., 2010. Influence of clay mineralogy on the stability of a landslide in Plio-Pleistocene clay sediments near Grassano (Sothern Italy). Catena 80 (2), 75–85.
U.S. Geological Survey, 2013. Landslide Hazards Program. landslides.usgs.gov.
Vannote, R.L., Minshall, G.W., Kummins, K.W., Sedell, J.R., Cushing, C.E., 1980. The river continuum concept. Can. J. Fish. Aquat. Sci. 37 (1), 130–137.
Varnes, D.J., 1978. Slope movement types and processes. In: Schuster, R.L., Krizek, R.J. (Eds.), Landslide Analysis and Control, Transportation Research Board, National Research Council, Special Report 176, Washington, DC, pp. 11–33.
Wilson, J.P., Gallant, J.C., 2000. Terrain Analysis: Principles and Applications. John Wiley and Sons, Inc., New York, NY (479 pp.).